A STUDY OF THE SURFACE HEAT-FLUX FLUCTUATIONS THROUGH DNS OF TURBULENT HEAT TRANSFER IN A CHANNEL FLOW

Hiroyuki Abe
CFD Technology Center,
National Aerospace Laboratory of Japan
Jindaiji-higashi, Chofu, Tokyo 182-8522, Japan
habe@nal.go.jp

Hiroshi Kawamura
Department of Mechanical Engineering,
Tokyo University of Science
Yamazaki, Noda-shi, Chiba 278-8510, Japan
kawa@rs.noda.tus.ac.jp

Yuichi Matsuo
CFD Technology Center,
National Aerospace Laboratory of Japan
Jindaiji-higashi, Chofu, Tokyo 182-8522, Japan
matsuo@nal.go.jp

ABSTRACT

In the present study, direct numerical simulation (DNS, hereafter) of turbulent heat transfer in a channel flow has been carried out in order to investigate the characteristics of the surface heat-flux fluctuations. The Reynolds numbers based on the friction velocity and the channel half width are 180, 395 and 640, and the molecular Prandtl numbers are 0.025 and 0.71. It is found that the large-scale structures exist even in the surface heat-flux fluctuations for both of the Prandtl numbers at high Reynolds number, which are essentially associated with large-scale motions for the thermal field existing in the outer layer. In addition, it is shown that the surface heat-flux fluctuations for the Prandtl number of $Pr = 0.71$ are mostly similar to the streamwise wall shear-stress fluctuations, but there exists the noticeable dissimilarity in the large positive and negative fluctuations.

INTRODUCTION

The behaviors of wall variables in the turbulent channel and boundary layer flows are of considerable interest in the application involving drag, noise and heat transfer. In the flow field, the studies of the wall shear-stress and pressure fluctuations through DNS have been made by several researchers (see, for example, Choi and Moin, 1990; Jeon et al., 1999). In the thermal field, the study of the surface heat-flux fluctuations through DNS has been performed by Kim and Moin (1989) for $Re_\tau = u_\tau \delta/\nu = 180$ at $Pr = 0.71$ with an assumption of constant heat generation throughout the fluid, where u_τ is the friction velocity, δ the channel half width, and ν the kinematic viscosity. However, they only reported the root-mean-square value and the instantaneous field, and the characteristics of the surface heat-flux fluctuations have not been investigated through DNS in detail.

Recently, with the rapid increase in the computer power, DNSs of turbulent channel flow have been carried out at relatively high Reynolds numbers (see, for example, Antonia and Kim, 1994; Moser et al., 1999; Abe et al., 2001). In addition, several large-scale DNSs have been performed at relatively high Reynolds numbers in a turbulent channel flow (del Álamo and Jiménez, 2001) and in a channel flow with turbulent heat transfer (Abe and Kawamura, 2002). Therefore, in the present study, we have extended DNS by Abe and Kawamura (2002) to investigate the characteristics of the wall variables such as the surface heat-flux fluctuations $q_w = a\rho c_p(\partial\theta'/\partial y|_w)$ up to $Re_\tau = 640$, where θ' denotes the temperature fluctuations, and y the distance from the wall. Note that a is the thermal diffusivity, ρ the density, and c_p the specific heat at constant pressure. The purpose of the present study is to report the behaviors of q_w from their root-mean-square values, power spectra, two-point correlations, probability density functions and instantaneous fields at the Reynolds number up to $Re_\tau = 640$ with $Pr = 0.025$ and 0.71. In addition, the dissimilarity in the wall variables for the flow and thermal fields is also investigated.

NUMERICAL PROCEDURES

The flow is assumed to be a fully developed turbulent channel flow with passive temperature field. It is driven by the streamwise mean pressure gradient. The temperature is imposed through the uniform heating on both walls. Note that the averaged heat flux is constant but the instantaneous one is time dependent. The present thermal condition corresponds to a heating (cooling) wall with an infinitely large thermal capacity and conductivity. For the spatial discretization, the finite difference method is adopted. The numerical scheme with the fourth-order accuracy is applied in the streamwise and spanwise directions, while the one with the second-order is adopted in the wall-normal direction. Further detailed method can be found in Kawamura et al. (2000) and Abe et al. (2001).

The computational domain size ($L_x \times L_y \times L_z$), number of grid points ($N_x \times N_y \times N_z$) and spatial resolution ($\Delta x \times$

Table 1: Domain size, grid points and spatial resolution

Re_τ	180	395	640
$L_x \times L_y \times L_z$	$12.8\delta \times 2\delta \times 6.4\delta$	$12.8\delta \times 2\delta \times 6.4\delta$	$12.8\delta \times 2\delta \times 6.4\delta$
$L_x^+ \times L_y^+ \times L_z^+$	$2304 \times 360 \times 1152$	$5056 \times 790 \times 2528$	$8192 \times 1280 \times 4096$
$N_x \times N_y \times N_z$	$256 \times 128 \times 256$	$512 \times 192 \times 512$	$1024 \times 256 \times 1024$
$\Delta x^+, \Delta y^+, \Delta z^+$	$9.00, 0.20 \sim 5.90, 4.50$	$9.88, 0.15 \sim 6.52, 4.94$	$8.00, 0.15 \sim 8.02, 4.00$

$\Delta y \times \Delta z$) are given in Table 1. A fairly large domain size is employed in order to contain a few numbers of large-scale structures. The accuracy with the present spatial resolution has been already confirmed by Kawamura et al. (2000) and Abe et al. (2001).

RESULTS AND DISCUSSION

Root-mean-square values

The rms values of the surface heat-flux fluctuations (q_w) normalized by the surface heat flux Q_w for $Re_\tau = 180$, 395 and 640 with $Pr = 0.025$ and 0.71 are given in Fig. 1. The streamwise wall shear-stress fluctuations ($\tau_1 = \mu(\partial u'/\partial y|_w)$) are also plotted for comparison, where u' denotes the streamwise velocity fluctuations and μ the dynamic viscosity. The present results for τ_1 agree well with those of other DNS and experiment. As for q_w, the values increase with increasing Reynolds number for both of the Prandtl numbers. The increasing rate for $Pr = 0.025$ is larger than the one for $Pr = 0.71$ because of the increasing convective effect. Here, it is interesting to mention that the rms value of q_w for $Pr = 0.025$ increases logarithmically with increasing Reynolds number. In addition, the rms values of q_w for $Pr = 0.71$ seems to increase more significantly than those of τ_{1rms}.

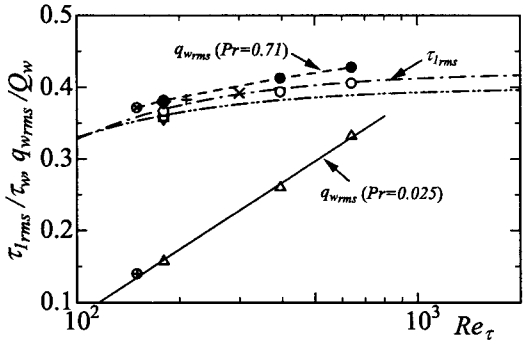

Figure 1: Variations of the rms values of the streamwise wall shear-stress τ_1 and surface heat-flux fluctuations q_w as a function of the Reynolds number. ○, τ_1; ●, q_w ($Pr = 0.71$); △, q_w ($Pr = 0.025$); ◇, Kim and Moin (1989); +, Gilbert and Kleiser (1991); ⊗, Kasagi et al. (1992); ⊕, Kasagi and Ohtsubo (1993); ▽, Antonia and Kim (1994); ×, Günther et al. (1998); □, Jeon et al. (1999); —·—, fitting for τ_{1rms}/τ_w by Fischer et al. (2001) from DNS; —··—, fitting for τ_{1rms}/τ_w by Fischer et al. (2001) from experiments; – – – –, fitting for q_{wrms}/Q_w ($Pr = 0.71$); ——, fitting for q_{wrms}/Q_w ($Pr = 0.025$).

Power spectra

The power spectra of q_w are defined as

$$\int_0^\infty \phi(k_x)dk_x = \int_0^\infty \phi(k_z)dk_z = q_{w\,rms}^2, \qquad (1)$$

where $\phi(k_x)$ and $\phi(k_z)$ are the power spectra, and k_x and k_z are the wavenumbers in the x and z directions, respectively. As was shown in Fig. 1, the mean-square values, i.e. integrations of the spectra over the wavenumber, increase with increasing Reynolds number. Accordingly, the streamwise- and spanwise-wavenumber power spectra of q_w are normalized by their own mean-square values with the inner scaling and are shown in Fig. 2. In the streamwise wavenumber power spectra, the spectra of q_w for $Pr = 0.71$ show a good collapse at the whole wavenumbers for all three Reynolds numbers, meaning that the contributions of small, intermediate and large scales in the streamwise direction to the rms values are essentially same at least for all three Reynolds numbers. Those of q_w for $Pr = 0.025$, on the other hand, collapse at small scale only, and exhibit an increase in power at large scales and a decrease in power at intermediate scales.

In the spanwise wavenumber power spectra, the spectra of q_w for both $Pr = 0.025$ and 0.71 show a collapse at small scales only, whereas they exhibit an increase in power at large scales with increasing Reynolds number (Fig. 2 (b)). This indicates that the contribution of large scales in the spanwise direction to the rms values increases with increasing Reynolds number and those of intermediate and small

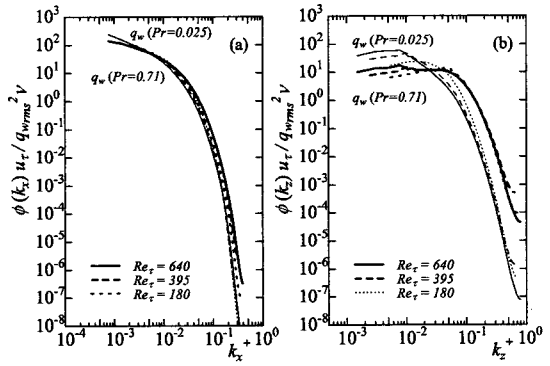

Figure 2: One-dimensional wavenumber power spectra of q_w normalized by the mean-square values with the inner scaling: (a) streamwise wavenumber; (b) spanwise wavenumber.

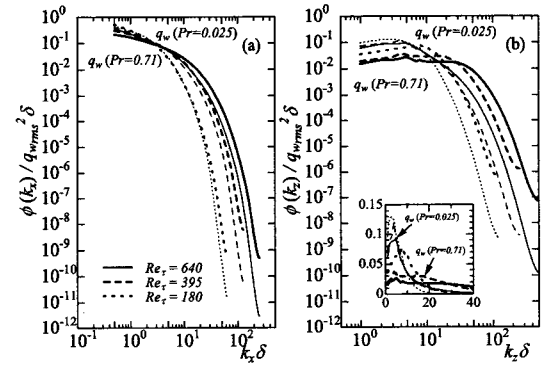

Figure 3: One-dimensional wavenumber power spectra of q_w normalized by the mean-square values with the outer scaling: (a) streamwise wavenumber; (b) spanwise wavenumber.

scales decrease to compensate for the increase in power at large scales.

The streamwise- and spanwise-wavenumber power spectra of q_w are normalized by their own mean-square values with the outer scaling and are shown in Fig. 3. In the case of $Pr = 0.71$, no collapse is found in the streamwise and spanwise spectra. In the case of $Pr = 0.025$, on the contrary, the streamwise and spanwise spectra show a good collapse at large scales, meaning that the contributions of large scales in the streamwise and spanwise directions to the rms values are same at least for all three Reynolds numbers.

Here, it is interesting to note that some peaks are observed at very low wavenumbers in the spanwise spectra (see Figs. 2(b) and 3(b)). The origin of these peaks must be closely related to large-scale motions (LSMs, hereafter) existing in the outer layer of the flow (see, for example, Robinson, 1991). In the inset figure (Fig. 3(b)), these low wavenumber behaviors are more clearly illustrated, where the power spectra are shown in linear scales. In the case of $Pr = 0.71$, there appear clear local peaks at $k_z\delta = 4 \sim 5$ at $Re_\tau = 395$ and 640, while a small bulge is observed at $Re_\tau = 180$. In the case of $Pr = 0.025$, on the other hand, large peaks are clearly observed at $k_z\delta = 4 \sim 5$ for all three Reynolds numbers. The wavelength corresponding to $k_z\delta = 4 \sim 5$ is $1.3 \sim 1.6\delta$ which is almost the same as the one found by Abe and Kawamura (2002) in the outer layer for the thermal field. This indicates that the large-scale structures in the outer layer maintain a certain influence even upon the inner layer quantities.

Two-point correlations

The streamwise and spanwise two-point correlations of q_w for $Re_\tau = 180$, 395 and 640 with $Pr = 0.71$ and 0.025 are given in Fig. 4 and 5, respectively. In the streamwise separation, there exist less Reynolds-number dependence when the two-point correlations for $Pr = 0.71$ and 0.025 are normalized by the inner and outer variables, respectively. This corresponds to the result of the streamwise wavenumber power spectra (see Figs. 2(a) and 3(a))

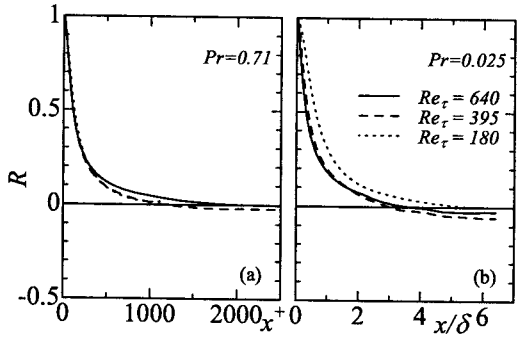

Figure 4: Streamwise two-point correlation coefficients of q_w: (a) $Pr = 0.71$; (b) $Pr = 0.025$.

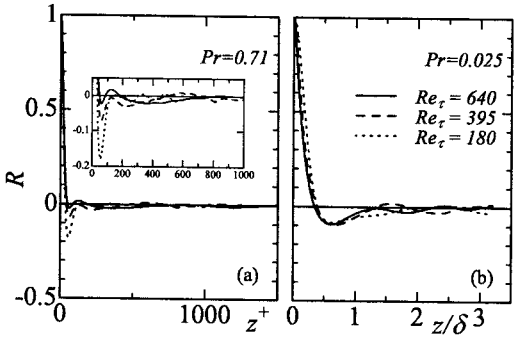

Figure 5: Spanwise two-point correlation coefficients of q_w: (a) $Pr = 0.71$; (b) $Pr = 0.025$.

In the spanwise separation, on the contrary, a significant Reynolds-number dependence is found at $Pr = 0.71$, while no prominent Reynolds-number dependence is observed at $Pr = 0.025$. That is, in the case of $Pr = 0.71$, the spanwise separation distance (in wall units) for maximum negative correlation is almost same for all three Reynolds numbers, but the magnitude of the negative maximum decreases appreciably with increasing Reynolds number. This behavior is consistent with the decrease in power in the spectrum of q_w at an intermediate wavenumber ($k_z^+ = 2\pi/\lambda^+ = 0.06$, where λ^+ is the streak spacing). In the case of $Pr = 0.025$, the spanwise separation distance for maximum negative correlation and the magnitude of the negative maximum are scaled with the outer variables. The negative maximum correlation is obtained at $\lambda_z/\delta \approx 0.65$, indicating that large-scale structures with a spanwise spacing of about 1.3δ exist even at the wall.

Probability density function

The behavior of the surface heat-flux fluctuations q_w is investigated with the use of the probability density functions (PDFs). Figure 6 shows the PDFs of q_w for all three Reynolds numbers of $Re_\tau = 180$, 395 and 640 with $Pr = 0.025$ and 0.71 as compared to those of τ_1. It is found in Fig. 6 that the sweep motion occurs less frequently but it contributes more significantly to the heat transport for both of the Prandtl numbers. The Reynolds-number effect is found in the positive and negative tails of the PDFs for both of the Prandtl numbers. In addition, a comparison of Figs. 6(a) and 6(b) reveals that the PDFs of q_w for $Pr = 0.71$ are mostly similar to those of τ_1, but there exists some dis-

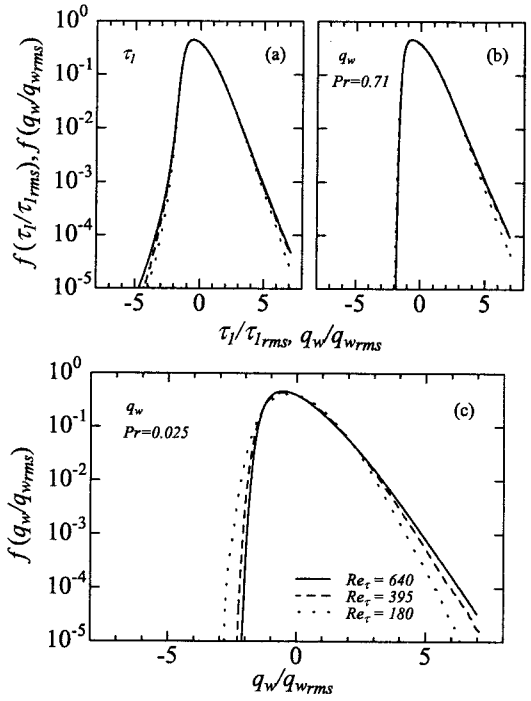

Figure 6: Probability density functions of the streamwise wall shear-stress and surface heat-flux fluctuations: (a) τ_1; (b) q_w for $Pr = 0.71$; (c) q_w for $Pr = 0.025$.

similarity between τ_1 and q_w at positive and negative tails. That is, in the positive tail, the PDF of q_w for $Pr = 0.71$ is larger than that of τ_1, indicating that q_w is more positively skewed than τ_1 in space. This trend corresponds to the measurement in the turbulent boundary layer by Antonia et al. (1988). In the negative tail, on the contrary, an interesting behavior is clearly observed, that is, the PDF of τ_1 extends to $\tau_1/\tau_{1rms} = -5$, whereas that of q_w stays within $q_w/q_{w_{rms}} = -2$. This point will be discussed later in the instantaneous fields.

In order to examine the correlations between flow and thermal fields, the joint probability density function between τ_1 and q_w is given in Fig. 7. In the case of $Pr = 0.71$, the strong positive correlation between τ_1 and q_w is found, whereas, in the case of $Pr = 0.025$, q_w less correlates with τ_1 due to the strong conductive effect. It is also found in Fig. 7 that the correlations at the high magnitude of the fluctuations decrease with increasing Reynolds number for both of the Prandtl numbers. Moreover, a closer inspection for $Pr = 0.025$ indicates that the maximum value in the third quadrant shifts away from the origin with increasing Reynolds number. This is caused by the enhanced convective effect even in the low Pr fluid.

Instantaneous fields

Figures 8(a) and 8(b) show the contours of the instantaneous surface heat-flux fluctuations q_w for $Re_\tau = 640$ with $Pr = 0.71$ and 0.025 in the full computational domain. For $Pr = 0.71$, it is found in Fig. 8(a) that the thermal streaky structures become more complicated for $Re_\tau = 640$, and they exhibit the dense clustering structures, that is, the negative q_w's are packed together and make a group in space. These behaviors correspond to the trend of the spanwise two-point correlations (Fig. 5(a)). Moreover, the dense clustering of negative q_w's clearly exhibits a large-scale pattern. For $Pr = 0.025$, on the contrary, it is found in Fig. 8(b) that the thermal structures scaled with the outer variable δ are dominant, corresponding to the result of the large negative maximum values in the spanwise two-point correlations (Fig. 5(b)).

To inspect the large-scale pattern of q_w at $Pr = 0.71$ in more detail, a filtering procedure with the use of a top-hat filter function is applied to the instantaneous field. A top-hat filter defined as

$$\widetilde{q_w}(x,z) = \frac{1}{4\ell_x\ell_z}\int_{-\ell_x}^{\ell_x}\int_{-\ell_z}^{\ell_z} q_w(x+\xi, z+\zeta)d\zeta d\xi \qquad (2)$$

is employed, where a tilde denotes a filtered value. Referring to Komminaho et al. (1996), the streamwise filter length ℓ_x is chosen as the integral scale and the spanwise filter length ℓ_z is roughly the same length as the first zero-crossing point of the spanwise two-point correlation. The filtered instantaneous field with $\ell_x^+ = 216$ and $\ell_z^+ = 48$ is shown in Fig. 8(c), where large-scale patterns with a spanwise spacing

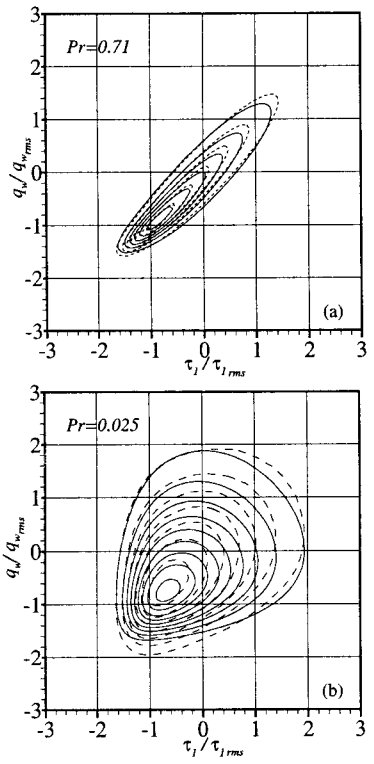

Figure 7: Joint probability density functions of the streamwise wall shear-stress and surface heat-flux fluctuations at $Re_\tau = 640$: (a) $Pr = 0.71$; (b) $Pr = 0.025$. ——, $Re_\tau = 640$; – – – –, $Re_\tau = 180$. Contour levels for $Pr = 0.71$ are from 0.1 to 0.6 with increments of 0.1, while those for $Pr = 0.025$ are from 0.025 to 0.225 with increments of 0.025.

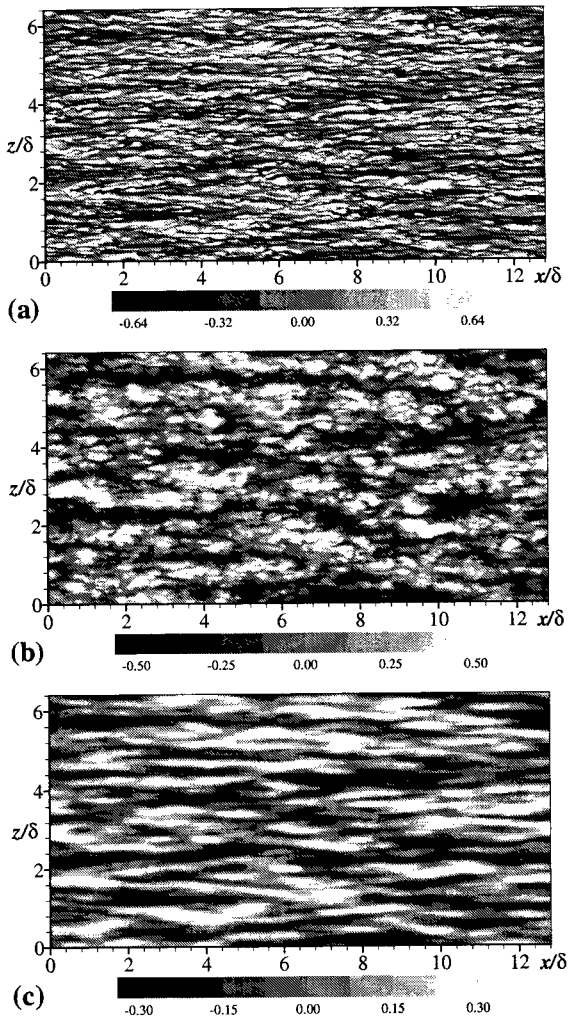

Figure 8: Contours of the instantaneous surface heat-flux fluctuations q_w for $Re_\tau = 640$: (a) instantaneous field at $Pr = 0.71$; (b) instantaneous field at $Pr = 0.025$; (c) filtered field at $Pr = 0.71$.

of about $1.3 \sim 1.6\delta$ (about 1000 in wall units for $Re_\tau = 640$) are more clearly illustrated. This spanwise spacing of $1.3 \sim 1.6\delta$ corresponds to the spanwise wavenumber of $k_z\delta = 4 \sim 5$ (or $k_z^+ = 0.006 \sim 0.008$) at which the spectrum of q_w shows a local maximum for $Re_\tau = 640$ (see Figs. 2(b) and 3(b)).

To examine the interaction between the inner and outer layers quantitatively, we introduce a function called an overlap ratio (OLR). In the OLR, variables ϕ and ψ are binarized to be either 0 or 1 based on a certain threshold, and the binarized ones are represented by $\hat{\phi}$ and $\hat{\psi}$. Then, the OLR is defined as the ratio of the overlapping area between $\hat{\phi}$ and $\hat{\psi}$ to the area of either $\hat{\phi}$ or $\hat{\psi}$:

$$\mathrm{OLR}(\phi < \phi_0 \text{ or } \phi > \phi_0 \mid \psi < \psi_0 \text{ or } \psi > \psi_0) = \sum \hat{\phi}\hat{\psi} / \sum \hat{\psi}^2, \quad (3)$$

where ϕ_0 and ψ_0 are the threshold values. We obtain the OLR between the filtered q_w (i.e. $\widetilde{q_w}$) and the projected area of high or low regions of θ' in the LSMs. First, $\widetilde{q_w}$ is binarized with a threshold of $\widetilde{q_w}_0/\widetilde{q_w}_{rms} = \pm 1.5$. Next, the high and low regions are binarized with respect to $\theta'_0/\theta'_{rms} = \pm 1.75$, and the binarized values are projected onto the wall and then re-binarized as 0 or 1. Through these procedures, the following OLRs can be obtained. The obtained OLRs between the high- and low-temperature regions in the LSMs and the positive and negative regions of q_w for $Re_\tau = 640$ with $Pr = 0.71$ are

$$\begin{aligned}
&\mathrm{OLR}(\theta' < -1.75\theta'_{rms} \mid \widetilde{q_w} < -1.5\widetilde{q_w}_{rms}) = 0.75,\\
&\mathrm{OLR}(\theta' < -1.75\theta'_{rms} \mid \widetilde{q_w} > \ \ 1.5\widetilde{q_w}_{rms}) = 0.30,\\
&\mathrm{OLR}(\theta' > \ \ 1.75\theta'_{rms} \mid \widetilde{q_w} > \ \ 1.5\widetilde{q_w}_{rms}) = 0.68,\\
&\mathrm{OLR}(\theta' > \ \ 1.75\theta'_{rms} \mid \widetilde{q_w} < -1.5\widetilde{q_w}_{rms}) = 0.21,
\end{aligned}$$

whereas the OLRs for $Re_\tau = 640$ with $Pr = 0.025$ are

$$\begin{aligned}
&\mathrm{OLR}(\theta' < -1.75\theta'_{rms} \mid \widetilde{q_w} < -1.5\widetilde{q_w}_{rms}) = 0.73,\\
&\mathrm{OLR}(\theta' < -1.75\theta'_{rms} \mid \widetilde{q_w} > \ \ 1.5\widetilde{q_w}_{rms}) = 0.06,\\
&\mathrm{OLR}(\theta' > \ \ 1.75\theta'_{rms} \mid \widetilde{q_w} > \ \ 1.5\widetilde{q_w}_{rms}) = 0.85,\\
&\mathrm{OLR}(\theta' > \ \ 1.75\theta'_{rms} \mid \widetilde{q_w} < -1.5\widetilde{q_w}_{rms}) = 0.06.
\end{aligned}$$

These results clearly indicate that the large-scale structures observed in q_w are essentially associated with the LSMs for the thermal field existing in the outer layer.

As was shown in the probability density functions, there exists some dissimilarity between τ_1 and q_w with $Pr = 0.71$ in the large positive and negative tails. Especially, the large negative tails showed the noticeable difference. This difference must be closely associated with the large wall pressure fluctuations. Therefore, we will examine the statistical quantities related to the wall pressure fluctuations such as $\overline{\tau_1 p_w}$ and $\overline{q_w p_w}$, where p_w denotes the wall pressure fluctuations. The resultant values of $\overline{\tau_1 p_w}$ for $Re_\tau = 180$ and 640 are 0.05 and 0.10, whereas those of $\overline{q_w p_w}$ for $Re_\tau = 180$ and 640 are -0.05 and -0.11, respectively. Here, it is interesting to mention that the values of $\overline{\tau_1 p_w}$ are positive, whereas those of $\overline{q_w p_w}$ are negative for both of the Reynolds numbers.

In order to examine the difference in $\overline{\tau_1 p_w}$ and $\overline{q_w p_w}$ with $Pr = 0.71$ in detail, the quadrant analysis is adopted. Fractional contribution and probability distribution of $\overline{\tau_1 p_w}$ and $\overline{q_w p_w}$ from each quadrant for $Re_\tau = 180$ and 640 are summarized in Tables 2 and 3. Note that $(\overline{\tau_1 p_w})_j$ and $(\overline{q_w p_w})_j$ are the fractional contribution from the jth quadrant and $P(\overline{\tau_1 p_w})_j$ and $P(\overline{q_w p_w})_j$ are the probability of the jth quadrant. It is indeed found that the contributions to $\overline{\tau_1 p_w}$ are more significant in the first ($\tau_1 > 0, p_w > 0$) and third ($\tau_1 < 0, p_w < 0$) quadrants for both of the Reynolds numbers, which causes the positive value in $\overline{\tau_1 p_w}$. Those to $\overline{q_w p_w}$, on the other hand, are in the second ($q_w < 0, p_w > 0$) and fourth ($q_w > 0, p_w < 0$) quadrants, which causes the negative value in $\overline{q_w p_w}$. These results indicate that the high

Table 2: Fractional contribution and probability distribution of $\overline{\tau_1 p_w}$ and $\overline{q_w p_w}$ at $Pr = 0.71$ from each quadrant for $Re_\tau = 180$

Event	$(\overline{\tau_1 p_w})_j$	$P(\overline{\tau_1 p_w})_j$	$(\overline{q_w p_w})_j$	$P(\overline{q_w p_w})_j$
$j=1$	0.10	0.23	0.08	0.21
$j=2$	-0.07	0.27	-0.10	0.29
$j=3$	0.10	0.29	0.08	0.27
$j=4$	-0.08	0.21	-0.11	0.23

Table 3: Fractional contribution and probability distribution of $\overline{\tau_1 p_w}$ and $\overline{q_w p_w}$ at $Pr = 0.71$ from each quadrant for $Re_\tau = 640$

Event	$(\overline{\tau_1 p_w})_j$	$P(\overline{\tau_1 p_w})_j$	$(\overline{q_w p_w})_j$	$P(\overline{q_w p_w})_j$
$j=1$	0.17	0.23	0.13	0.20
$j=2$	-0.10	0.27	-0.16	0.30
$j=3$	0.16	0.30	0.12	0.27
$j=4$	-0.13	0.20	-0.20	0.23

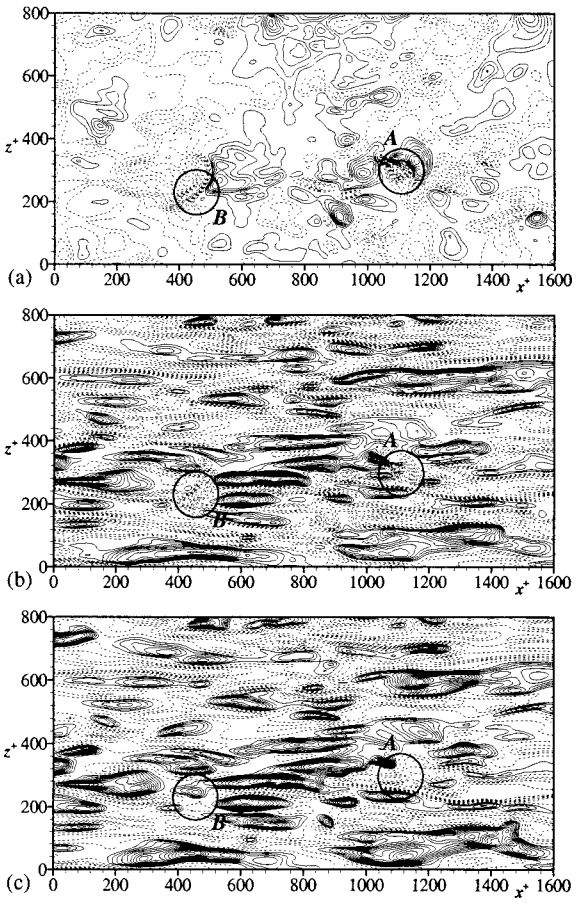

Figure 9: Contours of the instantaneous p_w, τ_1 and q_w with $Pr = 0.71$ for $Re_\tau = 640$: (a) p_w (contours are from -9.0 to 19.0 with increments of 1.0); (b) τ_1 (contours are from -1.3 to 1.9 with increments of 0.1); (c) q_w at $Pr = 0.71$ (contours are from -0.7 to 2.5 with increments of 0.1). Positive values are solid line, whereas negative values are dashed lines.

dissimilarity between τ_1 and q_w with $Pr = 0.71$ are closely associated with the wall pressure fluctuations.

The contours of the instantaneous p_w, τ_1 and q_w with $Pr = 0.71$ for $Re_\tau = 640$ are shown in Fig. 9. It is found in Fig. 9 that the positive and negative regions of q_w are mostly similar to those of τ_1. However, there exists the noticeable dissimilarity between τ_1 and q_w in the large pressure fluctuations. Especially, the dissimilarity is more clearly observed in the large negative p_w. In Fig. 9, the typical events of the dissimilarity are marked by A and B. In these events, the large negative regions of τ_1 correspond to those of p_w, which causes in the positive value of $\overline{\tau_1 p_w}$. On the contrary, the large positive and small negative regions of q_w to the large negative regions of p_w, which causes the negative value of $\overline{q_w p_w}$. Here, it should be noted that when the large negative τ_1 appears, the large negative p_w exists, but the reverse is not necessarily observed. In addition, it is interesting to mention that the magnitude of the negative q_w remains unchanged even in the large positive and negative p_w. These behaviors result in the large difference in the negative tails of the PDFs between τ_1 and q_w.

CONCLUSIONS

In the present study, we performed DNS of turbulent heat transfer in a channel flow with the constant time-averaged heat-flux boundary condition up to $Re_\tau = 640$ with $Pr = 0.025$ and 0.71, and investigated the characteristics of the surface heat-flux fluctuations.

It was found in the power spectra and two-point correlations that the surface heat-flux fluctuations for $Pr = 0.71$ are scaled well with the inner variables, whereas those for $Pr = 0.025$ are with the outer variables. It was also found in the spanwise wavenumber spectra that the peaks exist at the low wavenumbers for both $Pr = 0.025$ and 0.71 at high Reynolds number, suggesting that large-scale structures exist even in the surface heat-flux fluctuations.

The instantaneous fields showed that, in the case of $Pr = 0.71$, the large-scale structures with dense clustering pattern appear for high Reynolds number, whereas, in the case of $Pr = 0.025$, large-scale structures with the outer variable δ are dominant. In addition, the inspection of the interaction between inner and outer layers revealed that the positive and negative dominant regions in q_w correspond to the high- and low-temperature regions in the LSMs for both of the Prandtl numbers. These results indicate that the large-scale structures in the surface heat-flux fluctuations for $Re_\tau = 640$ are essentially the phenomena associated with the LSMs for the thermal field existing in the outer layer.

The examination of the dissimilarity between τ_1 and q_w for $Pr = 0.71$ showed that q_w are mostly similar to τ_1, but there exists the noticeable dissimilarity in the large positive and negative fluctuations. The closer inspection showed that the high dissimilarity between τ_1 and q_w exist in the large wall pressure fluctuations.

AKNOWLEDGEMENT

The present study is based on the former work on the wall shear stress fluctuations, in which a contribution by Prof. H. Choi of Seoul National University was significant. Computations were made with the use of VPP5000 at Tokyo University of Science and Computer Center of Kyushu University, and also Numerical Simulator III at Computer Center of National Aerospace Laboratory of Japan.

REFERENCES

Abe, H., Kawamura, H. and Matsuo, Y., 2001, " Direct numerical simulation of a fully developed turbulent channel flow with respect to the Reynolds number dependence," *ASME J. Fluids Eng.*, Vol. 123, pp. 382-393.

Abe, H. and Kawamura, H., 2002, " A study of turbulence thermal structure in a channel flow through DNS up to $Re_\tau = 640$ with $Pr = 0.025$ and 0.71, *Proc. of 9th European Turbulence Conference*, pp. 399-402.

Antonia, R. A. and Kim, J., 1994, " Low-Reynolds-number effects on near-wall turbulence," *J. Fluid Mech.*, Vol. 276, pp. 61-80.

Antonia, R. A., Krishnamoorthy, L. V. and Fulachier, L., 1988, " Correlation between the longitudinal velocity fluctuation and temperature fluctuation in the near-wall region of a turbulent boundary layer," *Int. J. Heat Mass Transfer*, Vol. 31(4), pp. 723-730.

Choi, H and Moin, P., 1990, " On the space-time characteristics of wall pressure fluctuations," *Phys. Fluids*, Vol. A 2, pp. 1450-1460.

del Álamo, J. C. and Jiménez, J., 2001, " Direct numerical simulation of the very anisotropic scales in a turbulent channel," *Center for turbulence Research Annual Research Briefs*, pp. 329-341.

Fischer, M., Jovanović, J. and Durst, F., 2001, "Reynolds number effects in the near-wall region of turbulent channel flows," *Phys. Fluids*, Vol. 13, pp. 1755-1767.

Gilbert, N. and Kleiser, L., 1991, " Turbulence model testing with the aid of direct numerical simulation results," *Proc. of the Eighth Symposium on Turbulent Shear Flows*, TU of Münich, pp. 26.1.1–26.1.6.

Günther, D. V., Papavassiliou, D. D., Warholic, M. D. and Hanratty, T. J., 1998, " Turbulent flow in a channel at low Reynolds number," *Exp. Fluids*, Vol. 25, pp. 503-511.

Jeon, S., Choi, H., Yoo, J. Y. and Moin, P., 1999, " Space-time characteristics of the wall shear-stress fluctuations in a low-Reynolds-number channel flow," *Phys. Fluids*, Vol. 11, pp. 3084-3094.

Kasagi, N., Tomita, Y. and Kuroda, A., 1992, " Direct numerical simulation of passive scalar field in a turbulent channel flow," *ASME J. Heat Transfer*, Vol. 144, pp. 598-606.

Kasagi, N. and Ohtsubo, Y., 1993, " Direct numerical simulation of low Prandtl number thermal field in a turbulent channel flow," In: *Turbulent shear flows 8*, Durst et al., eds., Springer-Verlag, Berlin, pp. 97-119.

Kawamura, H., Abe, H. and Shingai, K., 2000, " DNS of turbulence and heat transport in a channel flow with different Reynolds and Prandtl numbers and boundary conditions," In: *Proc. of 3rd Int. Symp. Turbulence, Heat and Mass Transfer*, Nagano et al., eds., pp. 15-32.

Kim, J. and Moin, P., 1989, " Transport of passive scalars in a turbulent channel flow," In: *Turbulent shear flows 6*, André et al., eds., Springer-Verlag, Berlin, pp. 85-96.

Komminaho, J., Lundbladh, A. and Johansson, A. V., 1996, " Very large structures in plane turbulent Couette flow," *J. Fluid Mech.*, Vol. 320, pp. 259-285.

Moser, R. D., Kim, J. and Mansour, N. N., 1999, " Direct numerical simulation of turbulent channel flow up to $Re_\tau = 590$," *Phys. Fluids*, Vol. 11, pp. 943-945.

Robinson, S. K., 1991, The kinematics of turbulent boundary layer, NASA TM 103859.